Oil Spill Detection Using Satellite Based SAR: Experience from a Field Experiment*

Abstract

During the commissioning phase of the ERS-1, C-band, synthetic aperture radar (SAR) images were obtained regularly over international waters for a range of operational, real-time uses. Among other capabilities, SAR is expected to be able to detect oil slicks on the sea surface. A project was defined with the aim of developing and demonstrating a system for early oil spill detection using satellite based SAR. During the Dedicated Oil Spill Experiment August 1991 (DOSE-91) three slicks, each 20 metric tons of stabilized crude oil, were released in phase with the passages of the ERS-1 satellite. The experiment included sea truthing, oil slick tracking using drifting buoys, and aircraft surveillance using various remote sensing techniques to compare and verify satellite observations. This paper presents the observations gathered during the experiment with emphasis on the SAR imagery of oil slicks under certain environmental conditions. Image enhancement techniques used to process the imagery are also discussed.

Introduction

Kasicscke *et al.* (1984) report on synthetic aperture radar's (SAR's) capability to detect oil slick. Among other samples, the report includes Seasat imagery of released oil from ships. The report does not indicate how the oil slick was verified or imaged by other techniques. Iguchi *et al.* (1988) reports on an experimental release of 180 litres of oleyl alcohol off the coast of Japan. The slick was imaged during the Shuttle Imaging Radar (SIR-B) mission in October 1984.

The ability of side-looking airborne radar (SLAR) to detect an oil slick on the sea surface has been accepted both by the scientific community and governmental agencies concerned with oil slick detection around the North Sea.

17 July 1991 marked the successful launch of the ERS-1 satellite combined with the ground segment's ability to deliver SAR data within rapid time frames, providing the opportunity to demonstrate the SAR's capability to detect oil under different environmental conditions, and to deliver the information to the scientific community in near real time.

In this paper we provide answers to the most critical questions related to the detection and monitoring of oil slicks from a satellite based Synthetic Aperture Radar (SAR):

- Is the ERS-1 satellite capable of detecting the oil?
- What are the detection capabilities relative to the operational airborne system?
- What are the major limits regarding detection?

Data Collection

Dedicated Oil Spill Experiment (DOSE-91)

The DOSE-91 experiment was undertaken in the period 19 August to 2 September with three oil releases on 21, 24, and 27 August. During each spill 20 metric tons of stabilized crude oil† were released on the sea surface in the planned released site: 63°30' North, 07°30' East. Figure 1 indicates the oil release site together with the buoy positions and the SAR track.

The experiment area was inspected and searched for species of guillemots and razorbills before the first oil release. When no large concentrations of razorbills or guillemots were found, operations proceeded with the planned release.

The oil slicks were mapped and traced by surface drifters, offshore field sampling, aircraft surveillance using SLAR and UV/IR, and by the ERS-1 satellite using full image mode SAR. The experiment area was instrumented with three oceanographic TOBIS buoys equipped with satellite positioning and data transmission systems. They measured wind and wave conditions.

Environmental Conditions During The DOSE-91 Experiment.

The following brief descriptions of the weather conditions in the area of the spill site for the period 21 August to 28 August are provided for later reference when SAR images are discussed in terms of prevailing environmental factors.

22 AUGUST

During the late morning of 22 August a warm front, associated with a low moving north eastwards from Iceland into the Norweigian Sea, passed over the spill site. Winds on the coast remained light (<5 m/s) throughout the day, starting variable in direction and settling towards the end of the day around southwesterly. Further offshore nearer the center of the low, winds were higher. The observations made on board

*Presented at the First Thematic Conference on Remote Sensing for Marine and Coastal Environments, New Orleans, Louisiana, 15-17 June 1992.

Tom-Ivar Bern
OCEANOR A/S, Pirsenteret, 7005 Trondheim, Norway
Terje Wahl
Norweigan Defence Research Establishment (NDRE), POB 25, N-2007 Kjeller, Norway.
Tom Anderssen
University of Oslo at Kjeller (UNIK), NDRE, POB 25, N-2007 Kjeller, Norway.
Richard Olsen
Satlantic Inc., Richmond Terminal-Pier 9, 3295 Barrington Street, Halifax, Nova Scotia, Canada B3K 5X8.

†Oil mixture: 35 percent Statfjord crude, 20 percent Gullfaks crude, and 45 percent DUC crude. The mixture did not develop a stable emulsion on the sea surface. On the 27 August release, 100 percent Statfjord was requested, 100 percent gullfaks was delivered.

Photogrammetric Engineering & Remote Sensing,
Vol. 59, No. 3, March 1993, pp. 423–428.

0099-1112/93/5903–423$03.00/0

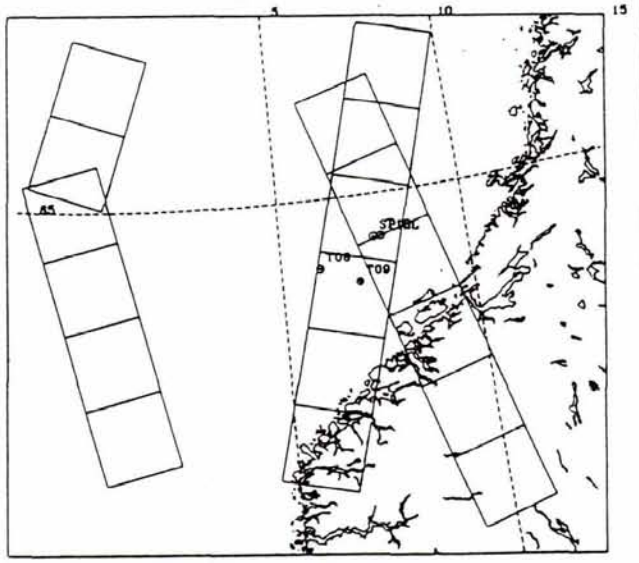

Figure 1. Map of experiment area with buoy positions and release site.

the *Svanaug Elise* at the oil spill site were considerably higher than on the coast, decreasing from 15 m/s at midday to 5 m/s soon after midnight. Significant wave height increased through the day to a peak of a little over 4 m at around 210 UTC in response to local wind and increasing swell, both from the south south-west. Peak wave period was around 9 to 10 sec.

Figure 2. SAR image from 25 August.

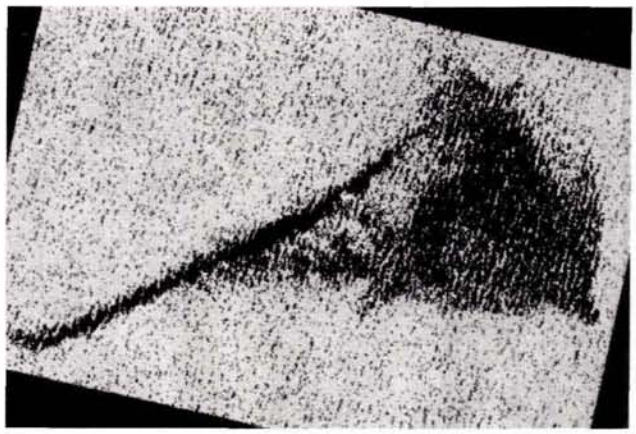

Figure 3. Thresholded oil slick from 25 August, T_{Opt} = 23.2 (FRI).

22 August

The low continued to move away northwards. Winds became even lighter at the coast on 22 August, but remained somewhat higher offshore (5 to 7.5 m/s), becoming southerly as the day progressed. Wave height continued to decrease, being around 2.8 m during the satellite pass with an 11-sec peak period. Wave direction was probably west to northwesterly for the swell while wind sea was more southerly.

24 August

Early on 24 August wind speed was around 10 m/s from the west at the oil spill location and wave height had reached a new peak of about 3 m associated with low pressure to the north. Both wind speed and wave height decreased as the day progressed. At the time of the SAR measurement wind speed was about 6 m/s from the northwest, significant wave height was a little over 1 m with a peak period of 6 to 7 sec. indicating wind sea dominated conditions from the north-

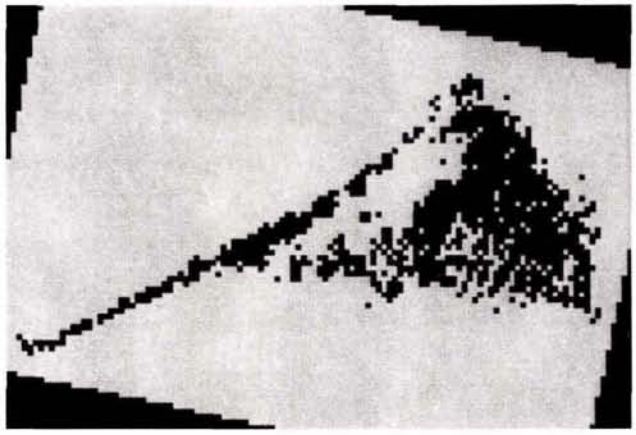

Figure 4. Thresholded oil slick from 25 August, T_{Opt} = 23.2 (LRI).

west. Slight swell from the northwest and southwest may also have been present.

25 AUGUST

On 25 August a fairly powerful low had developed off the southeast coast of Greenland and was moving slowly northeastwards. There were quite strong winds over Iceland and the western Norwegian Sea, but in the Haltenbanken area, winds remained weak throughout the day at about 2.5 m/s with variable direction. Wave height did, however, increase somewhat to a little over 2 m in the middle of the day at about the time when the SAR image was taken, with a peak period of a little over 10 sec. It is uncertain concerning the source of the swell which caused this increase, but it may have been the low which was located further north the day before.

27 AUGUST

Winds remained low on 26 August. However, a cold front associated with the aforementioned low, which was now at about 75°N on the coast of Greenland, moved past mid-Norway, bringing with it much stronger westerly winds on 27 August leading to increasing wave heights, between 3 and 4 m after midday with a peak period of around 13 sec. Wind speed reached a peak of about 12 to 13 m/s (strong breeze) at about the same time, winds and waves being predominantly southwest to westerly.

28 AUGUST

High pressure had built up over the North Sea on 28 August and fairly strong southwesterly winds continued to dominate the oil spill site, although turning more southerly later in day. Wind speed was probably in the region of 8 to 10 m/s throughout the day, significant wave height ranging from 2.6 to 3.6 m and still from the west-southwest.

Figure 5. Lee filtered SAR image from 25 August.

SAR Imaging Characteristics

In SAR image mode, the Active Microwave Instrument (AMI) on board the ERS-1 will obtain strips of high resolution imagery 100 km in width to the right of the satellite sub track. The 10-m long antenna is aligned parallel with the satellite orbit to direct a narrow radar beam sideways and downwards onto the Earth's surface over the 100-km swath. Imagery is built up from the strength of the return signal, which depends primarily on the roughness and dielectric properties of the surface.

Operation in SAR image mode is exclusive of other AMI operating modes, and power considerations limit operating time to a maximum of 10 minutes per orbit. The data rate is too high to allow on-board storage, so images can only be obtained within the reception zone of a suitably equipped ground station. The image mode technical specifications are listed in Table 1.

The problem of detecting an oil slick in a SAR image is threefold: the visibility of the oil slick in the SAR image under varied environmental conditions; the variation of SAR signatures from different oil types and different ages of the slick; and discrimination between oil slicks and other features in the SAR image (called "oil slick look-alikes").

Visibility of the oil slick in the SAR image depends upon the reduced radar backscatter from the sea surface. This backscatter is dependent upon the local wind speed. From the experience of this and other experiments carried out in Norway, image resolution during a range of wind speeds can be outlined as follows:

0 m/s	No backscatter from the undisturbed sea surface, hence no signature of oil slicks.
3 m/s	Excellent perturbation of the slightly roughened sea surface, no impact from the wind on the oil slick. However, a high probability of local low wind speed areas, providing oil slick "look-alikes."
3 to x m/s	Better conditions relative to false alarms from local low wind areas. The oil slick will still be visible and the background would be more homogeneous.
> x m/s	The oil slick will be invisible due to a combination of oil slick dispersion, which depends upon the oil type, wave breaking, and velocity bunching. Velocity bunching is primarily a wave height and wave period driven mechanism. x is a variable depending on oil type, and slick age, i.e., time since release. An upper limit for detection was found at wind speed 6 m/s for the oil type used during the DOSE-91 experiment.

Oil slick "look-alike" features in the SAR image can be interpreted as oil slicks, but are the results of other oceanographic or meteorological phenomena. Oil slick "look-alikes" are most likely either areas of low wind speed and hence backscatter, or areas of natural films from micro-organisms. Both oil slicks and oil slick "look-alikes" are found in the SAR image of 25 August (Figure 2). Look-alike features can also probably be other phenomena that require more documentation.

Several profiles in the SAR image of 25 August have been made starting with filtering the data with a 5 by 5 averaging filter. Conclusions drawn from this discussion are based on this low resolution imaging technique. Assumptions included that there were differences in the transition zones from the undisturbed sea to the dark feature discriminating the oil slick from the "look-alike" and that the signal variation within the slick differed from the variation within the slick "look-alike."

However, no large differences in the transition zones between the oil slicks and the undisturbed sea surface compared to the transition zones of an oil slick "look-alike" were found. Neither were there significant signal variations between the radar backscatter from the 25 August oil slick and the "look-alike."

Filtering of Selected ERS-1 SAR Scenes from the DOSE-91 Experiment

Several micro-scatterers make random contributions to the reflected signal within one ground resolution cell. SAR imaging of homogenous ocean areas is therefore degraded with speckle. The presence of speckle will, in general, make detection of objects more difficult. For this reason, most ERS 1 SAR processors make use of multilook techniques (where different parts of the total aperture are processed separately, followed by incoherent addition). The three-look method used in standard ERS-1 images is not sufficient for full removal of speckle, however, and thus additional filtering is often required. This section reviews some selected ERS-1 scenes from DOSE-91. One especially interesting scene (25 August) is investigated in some detail. Some classical edge detection algorithms were tested, in addition to 5 by 5 averaging, histogram analysis, and Lee filter techniques. The SAR processing was done by the European Space Agency (ESA).

Early work on oil slicks occasionally seen in SAR images favored the use of the low resolution ERS-1 SAR product from Tromsø Satellite Station for oil slick detection, as this image format has sufficient resolution for oil slicks, a very good radiometric resolution, and a size (2.5 MByte) that can be easily handled for rapid distribution.

TABLE 1. IMAGE MODE TECHNICAL SPECIFICATIONS

Frequency:	5.2 GHz (C-band)
Polarization:	VV
Incidence angle:	23°
Spatial resolution	30 m
Radiometric resolution	2.5 dB at −18dB
Swath width	100 km
Data rate	<105 Mbps

Averaging Filter

Because of speckle, simple thresholding in a full resolution SAR image will usually not be a good method for segmentation of oil slicks. Averaging will reduce the speckle and, thus, make thresholding techniques better suited. A major advantage of averaging is that the same statistical distribution function can be used, except for an increased number of effective looks. It was foreseen by Tromsø Satellite Station that 5 by 5 averaged ERS-1 images could be of interest in various applications. Thus, the SAR processor at Tromsø auto-

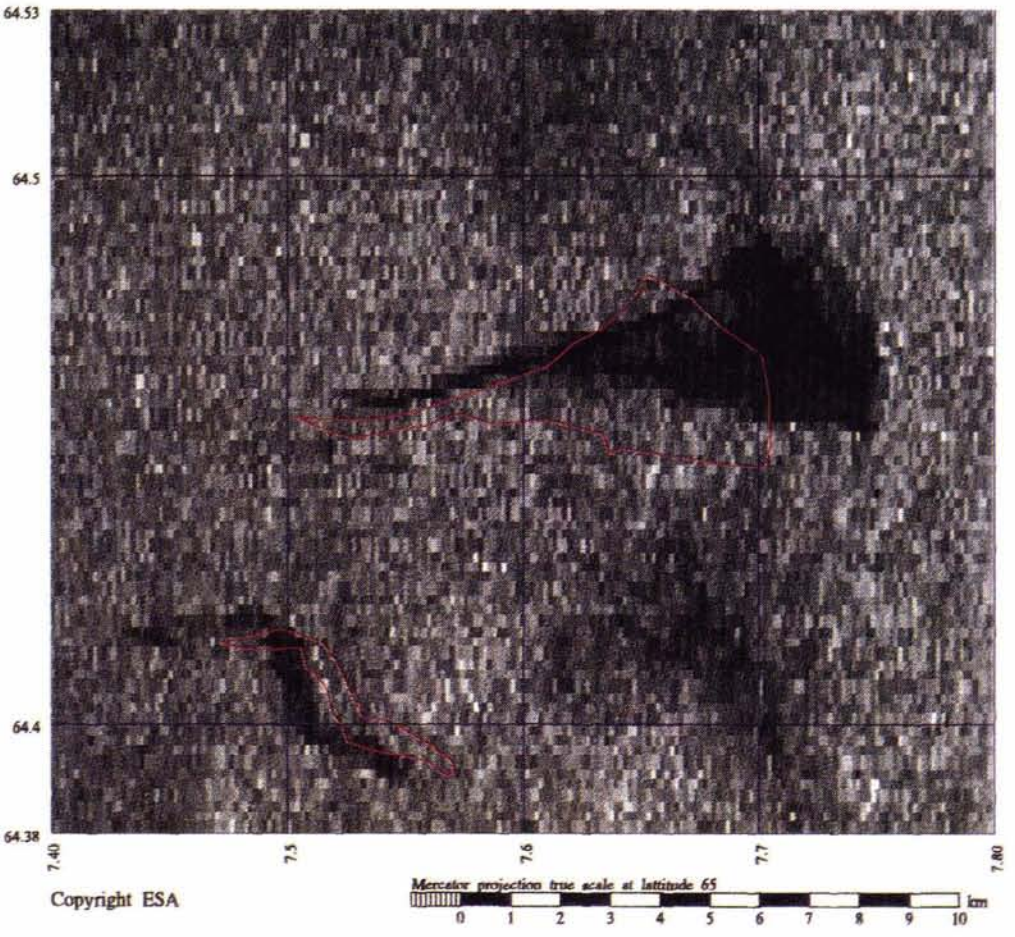

Plate 1. Extract of SAR image from 25 August with overlaid SLAR oil slick outlines.

matically produces a low resolution (100 m) averaged image in addition to the full resolution image (FRI).

By averaging 5 by 5 pixels from the FRI we have obtained a low resolution image (LRI) similar to those produced by the Tromsø Satellite Station.

The speckle distribution in amplitude images can be modeled by a Gamma distribution (Ulaby *et al.*, 1986) given as

$$P(s) = 2q\frac{M^M}{(M-1)!}\left(q\frac{S}{\mu}\right)^{2M-1} e^{-M\left(q\frac{S}{\mu}\right)^2}\cdot q = \frac{\Gamma(M+0.5)}{\sqrt{M}\,\Gamma(M)} \quad (1)$$

where μ is the mean value of the distribution and M is the number of looks.

To see how the empirical histogram matches the theoretical one, they were plotted together from some selected areas in the image. Analysis of real ERS-1 data shows that Equation 2 is a good description of the SAR speckle.

By using estimated values from two slicks in the FRI, an optimal threshold for segmentation was determined. The mean value of the oil slick has been measured to $\mu_{Oil}=12.6$, the mean sea backscatter to $\mu_{Sea}=49.4$ and $M_{Eff}=1.7$. Due to the large oil-sea difference (12 dB), a certain bimodality was observed even in the FRI. Minimizing the error by thresholding results in an optimal threshold, T_{Opt}, as given below:

$$T_{Opt} = \sqrt{\frac{\ln(k)}{Mq^2\left(\frac{1}{\mu_{Sea}^2}-\frac{1}{\mu_{Oil}^2}\right)}}, \qquad k = \frac{1-a}{a}\left(\frac{\mu_{Oil}}{\mu_{Sea}}\right)^{2M} \quad (2)$$

An optimal threshold for the oil slick, given the measured data, is $T_{Opt}=23.2$. The result by applying this threshold is shown in Figure 3. Similar calculations in the LRI resulted in $T_{Opt}=21.8$, and the threshold image is shown in Figure 4. By averaging, the segmentation performance has improved significantly, as very good separation of the oil and the sea pixels in the histogram has been achieved. Comparing the two segmented images, nearly all of the surrounding black pixels in Figure 3 have been correctly segmented as sea pixels in Figure 4.

Classical Edge Enhancement Filters

The performance of some edge-enhancement filters have been tested, including the gradient filter, the Sobel filter, and an adaptive Sobel filter.

None of these filters gave promising results due to the heavy noise characteristics.

The Lee Filter

Adaptive filters have been experimented with as a useful tool for reducing the speckle noise in SAR imagery for some time. Most of the literature, however, discusses application to imagery of land features. The main problem with traditional approaches to speckle noise reduction in SAR imagery is that standard forms of averaging or low-pass filtering result in reduced spatial resolution. Ideally, a filter should preserve the radiometric information which contains the underlying geophysical signal, including edges and textures, while removing the non-geophysical variance related to the radar interference pattern. Adaptive filters try to accomplish this by assuming that a valid model may be formulated for the noise variance in a homogenous area, and comparing this with the actual variance observed in a segment of the imagery. If the model agrees with the observed value, the area is assumed to be homogenous, and relative heavy smoothing is applied. If the variance is higher than the model predicts, it is assumed that there is an underlying geophysical feature which should be preserved, and less smoothing is applied. This, however, is carried out in different ways in different filters, depending on the model assumptions.

In this study the Lee filter (Lee, 1980; Lee, 1983) was examined. The filter is based on the assumption that the observed pixel value I(x,y) may be expressed as

$$I(x,y) = R(x,y)\cdot u(x,y) \quad (3)$$

where R is the stationary random process which describes the terrain reflectivity, u is the multiplicative noise due to fading, and (x,y) is a location in the image. This may be modeled as a stationary white non-Gaussian random process with a χ^2 distribution. Lee derived a Minimum Mean Square Error (MMSE) filter estimate which can be expressed by a weighted sum of the mean and observed image values: i.e.,

$$\hat{R}(x,y) = I(x,y)\cdot W(x,y) + \hat{I}(x,y)\cdot(1 - W(x,y)) \quad (4)$$

where $\hat{I}$ is the average image value within the filter window, I is the observed value at the window center, and the weighting functions W is

$$W(x,y) = 1 - \frac{C_u^2}{C_I^2(x,y)} \quad (5)$$

where C_u is a theoretical noise variation coefficient and C_I, the observed coefficient of variation, is $C_I = \sigma_I/I$ where σ_I is the observed standard deviation of the pixels in the filter window.

Other filters, such as the Frost, Kuan, and geometric filters, provide for different filter expressions. Lopes *et al.* (1990) have also proposed some modifications to several of these filters, which should improve their performance. It was beyond the scope of the project to investigate the utility of these filters. It would, however, be worthwhile to examine them in conjunction with other pre-processing techniques. The ERS-1 image from 25 August demonstrates this, where it is evident that a significant part of the image variance is related to ocean surface wave patterns. Removal of these by, for example, band pass filtering around the dominant wave length may prove to be an advantage.

Analysis of the Image from 24 August.

This image was acquired in relatively high wind and sea-state conditions. There is no evident wave pattern in the image, however. The Lee filter was applied with several different window sizes to a subimage containing the oil slick in order to determine which window size was most efficient in segmenting the oil slick from the surrounding sea. The objective measure was to see whether the filtering would separate the image histogram into two distinct peaks which could be used for separation of "oil slick pixels" from the surroundings. This, however, proved difficult, as many other areas in the image have the same low pixel values as the oil slick. Also, a number of bright points appear in the imagery, which are likely points of specular reflection, due to steep local incidence angle of the radar pulse and possible breaking of waves. A 3 by 3 square moving average algorithm was applied to the filtered image in order to remove some of these. In a somewhat subjective opinion, the best improvement was obtained with a 9 by 9 pixel Lee filter, followed by a 3 by 3 moving average.

Analysis of the Image from 25 August

This image has a clearly defined wave pattern present. The oil spill is also much more clearly defined. Again, the Lee filter was applied with several different window sizes. The separation of the darker oil spill pixels became more evident as the window size was increased. The larger size of the oil spill warranted a larger filter size, and we obtained best re-

sults with a 11 by 11 and 21 by 21 pixel size filter window. The resulting image of a 21 by 21 window filter is presented in Figure 5.

Synthesis of SAR and SLAR Data

The video signals from the SLAR and UV/IR data were recorded on board an aircraft using a Viewmaster video recorder. A PC with video frame grabber card was used to digitize SLAR images. The images were transferred for processing using a raw data format interpreting the data as 8-bit pixels.

The SLAR and SAR recording of 24 August was of low quality, i.e., the oil slick was hardly discernible from the surrounding sea. However, the results confirmed the observations made on the 25 August imagery.

In the processing of a raster image, at least four fix points must be given with known raster coordinates and geographical coordinates in order to estimate the parameter of the transformation. For geopositioning of the SLAR recording on 25 August, the aircraft position, the two end points of the slick, and the position of *Svanaug Elise* were used. Using this geopositioned image, the SLAR generated outline of the oil slick was recorded.

The SAR images from 24 and 25 August were transferred from the image processing system to the GIS system. Prior to the transfer, the data were filtered using a 5 by 5 block averaging filter. After the filtering, the cumulative distribution of the resulting 16-bit pixel values was calculated. Using the 98 percent threshold as an upper limit, an estimate of a linear scaling from 16 bit to 8 bit using a constant factor was made. For the image recorded on 25 August, the factor ensuring 98 percent of the pixel variation to be in the range 0 to 255 was 0.092. The four corners of the SAR image were used to geoposition the image.

The outline of the oil slicks from the geopositioned SLAR image is superposed on the SAR image in Plate 1. We can note the following:

- The form of the slicks imaged by the SLAR and the SAR is highly correlated.
- The geopositioning of the outline of the slick is based on the aircraft navigation system, recorded by the video system, and the position of the boat. The geopositioning of the SAR image reference points is based on the predicted orbit. Even so, the maximum distance between the slick as detected by the SAR and the SLAR is 2.3 km.

Conclusions

During the DOSE-91, a small set of SAR images containing oil slick signatures was collected. These SAR images verify that the SAR on board the ERS-1 satellite is capable of detecting oil slicks. The signal strength of the oil slick signature in the SAR image is a product of the oil type, amount of spilled oil, and age of the slick. The clarity of the oil slick is also a product of the environmental conditions at the time of imaging.

The results from the experiment gave examples of situations in all three imaging regions: i.e., clear oil slick signatures in the SAR image, borderline situations with hardly detectable oil slicks, and also examples of SAR imagery which did not contain any oil slick signature. The differences in these situations are due to the wind and wave conditions varying throughout the experiment. The experience from DOSE-91 indicates that detection is primarily a function of wind speed. Detection threshold for the oil type used during the DOSE-91 campaign is a wind speed of 6 m/s.

Analysis of signatures after averaging filters were applied indicates that the speckle noise in the image was reduced, and the loss of resolution does not influence the ability to detect the slick.

Adaptive filtering of the data can yield added information to the image. However, in an operational system, the processing time using such filters might become prohibitive.

The accuracy of the geoposition information contained in the SAR image (Fast Delivery Product) is sufficient to provide a good estimate of the location of the detected slick. The satellite-based SAR and the aircraft SLAR have comparable oil slick detection limits.

Acknowledgement

The study on Oil Spill Detection has been undertaken on behalf of a group of interested parties. The work has been funded by ESSO Norge a.s., STATOIL Norge a.s., Marine Spill Response Corporation, Norweigian Space Centre, the Norwegian State Pollution Control Authority, the European Space Agency, Digital Equipment Corporation Norge A/S, and OCEANOR A/S.

The authors thank the Steering Committee and the sponsors for the valuable contribution both in the financing of the project and in the discussions on possibilities and limitations of the techniques available.

References

Bern, T.-I., and S. Moen, 1992. *Oil Spill Detection Using Satellite Based SAR*, Completion report for Phase 0 and 1, OCEANOR report no.: OCN-R92071

Iguchi, T, and H. Inomata, 1988. SIR-B Experiment in Japan; IV Experimental Results; 3. Oil-Pollution Experiment. *Journal of the Radio Research Laboratory*. Vol. 35, Special Issue No. 2, pp. 85-104.

Kasiscke, E.S., G.A. Meadows and P.L. Jackson 1984. *The Use of Synthetic Aperture Radar Imagery to Detect Hazards to Navigation*. ERIM Report No. 169200–2–F.

Lee, J.S., 1980. Digital Enhancement and Noise Filtering by Use of Local Statistics. *Comput. Graph. Image Proc.* Vol. 17, pp. 380-389.

1983. A Simple Speckle Removing Algorithm for Synthetic Aperture Radar Images. *IEEE Trans. Syst., Man., Cybern.* Vol. SMC-13, No. 1, pp. 85-89.

Lopes, A., Touzi, and E. Nezry, 1990. Adaptive Filters and Scene Heterogeneity. *IEEE Trans. Geoscience & Remote Sensing*. Vol. GRS-28, No. 6, pp. 992-1000.

Ulaby, F.T., F. Kouyate, B. Brisco, and T.H.L. Williams, 1986. Textural Information in SAR images. *IEEE Trans. on Geoscience and Remote Sensing*, Vol. GE-24, No. 2, March 1986. pp. 235-245.